



Electrochemical investigations and antimicrobial activity of Au nanoparticles photodeposited on titania nanoparticles

Hussein M.A. Al-Maydama^a, Yasmin M.S. Jamil^{a,*}, Mohammed A.H. Awad^{a,b}, Adlia A.M. Abduljabbar^c

^a Chemistry Department, Faculty of Science, Sana'a University, Yemen

^b Chemistry Department, Faculty of Applied Sciences, Thamar University, Yemen

^c Chemistry Department, Faculty of Applied Sciences and Humanities, Amran University, Yemen

ARTICLE INFO

Keywords:

TiO₂ nanoparticles
Anodization
Au nanoparticles
Photodeposition
Glycerol electrooxidation
Cyclic voltammetry
Antimicrobial activity

ABSTRACT

Titanium oxide nanopowder (TiO₂ NPs) was synthesized via anodization in 0.7 M perchloric acid then annealed in nitrogen at 450 °C for 3 h to prepared the Titanium Oxide Nitrogen annealed nanoparticles (TiO₂ NPs-N₂) powder as catalytic support. Using a photodeposition process, gold was added with isopropanol as a sacrificial donor and H[AuCl₄] acid, producing gold nanoparticles on nitrogen-annealed titanium oxide nanoparticles (Au-NPs on TiO₂-NPs-N₂). The mass loading of Au NPs was 2.86×10^{-4} (g/cm²). TEM images of Au NPs on TiO₂-NPs-N₂ suggest circular particles with a tendency to agglomerate. Cyclic voltammetry (CV) was used to investigate the electrocatalytic performance of the Au NPs/TiO₂-NPs-N₂ catalysts in ferrocyanide, KOH, and H₂SO₄, and the results were compared to those of a polycrystalline Au electrode that is readily accessible in the market. In KOH, H₂SO₄, and (2 M KOH + 0.1 M glycerol) solutions, the Au NPs/TiO₂-NPs-N₂ electrode displayed a startlingly high electrocatalytic performance. Using CV, the electrocatalytic oxygen reduction reaction (ORR) of Au NPs/TiO₂-NPs-N₂ and Au-NPs against glycerol oxidation in basic media was studied. The results indicated that Au NPs/TiO₂-NPs-N₂ is a promising support material for improving the electrocatalytic activity for acidic and basic oxidation. The electrode made of Au NPs/TiO₂-NTs-N₂ has steady electrocatalytic activity and may be reused repeatedly. TiO₂ NPs and Au NPs/TiO₂NPs-N₂ showed satisfactory antibacterial activity against some human pathogenic bacteria using the disc diffusion method.

1. Introduction

Owing to their multiple uses in heterogeneous catalysis, nanoparticles of noble metals placed on metal oxides have attracted the interest of several researchers over the past few decades [1]. Applications for metal nanoparticles supported on the semiconductor surface of a metal oxide include wastewater treatment, purification, medicine, photocatalytic production of solar fuel, and industrial photocatalysis processes [2]. According to Wenderich & Mul (2016), nanoparticles can significantly enhance the functioning and constancy of semiconductors in operations initiated by the absorption of energy from light. When loaded properly, catalyst nanoparticles can serve as (i) charge carriers upon photoexcitation, inhibiting electron/hole recombination, (ii) active sites for processes including charge transfer, and (iii) enhanced absorption of light, especially for Au and Ag [2].

* Corresponding author.

E-mail address: y.jamil@su.edu.ye (Y.M.S. Jamil).

<https://doi.org/10.1016/j.heliyon.2023.e23722>

Received 17 August 2023; Received in revised form 9 December 2023; Accepted 12 December 2023

Available online 19 December 2023

2405-8440/© 2023 Published by Elsevier Ltd.

This is an open access article under the CC BY-NC-ND license

(<http://creativecommons.org/licenses/by-nc-nd/4.0/>).

During the last few decades, in the area of environmental growth, semiconductor nanomaterials have initiated an excellent curiosity in researchers on account of the exceptional physicochemical characteristics, including nontoxicity and environmental sustainability [3]. Recently, advancements in the field of nanotechnology have attracted significant attention for nanomaterials (NMs) owing to their higher surface area-to-volume percentage in comparison to bulk, with sizes in nanometers (1–100 nm), resulting in an outstanding increase in catalytic and biological activity [4]. Recently, nanostructures such as zero-dimensional (0D), one-dimensional (1D), two-dimensional (2D), and three-dimensional (3D) nanostructures have attracted particular attention owing to their unique properties and potential for innovative applications [5,6].

The surface area of the electrodes increases when nanomaterials are used to alter them, increasing their ability to sense the electrochemical biosensor. This is now well recognized. Because of this, several possible electrode applications have been modified with nanomaterials, including energy-conversion technologies, biochemical sensors, and catalysis [7–10]. In this context the most used nanomaterials nowadays are carbon derivatives (carbon nanotubes (CNT), graphene oxide (GO), etc.) [11,12], metallic nanoparticles (as Ag, Au, and Cu) [13,14], carbon derivatives and their hybrids [15–17] are currently the majority of frequently used nanomaterials in this field. Owing to their electronic, optical, and magnetic properties, gold nanoparticles have received considerable attention [18, 19]. Au NPs also increase electron transport and strengthen analytical sensibility [20]. Therefore, the electro catalytic activity of Au NPs is affected by their shape and size [21–23], the synthesis process and technique of electrode surface immobilization must be carefully managed.

Because of the relatively slow kinetics of oxygen generation and breakdown on most electrodes, the oxygen reduction reaction (ORR) considerably restricts the wide-ranging use of fuel cells [24]. In these applications, platinum (Pt) and its alloys are primarily employed as anodic and cathodic catalysts, but this metal is expensive and has a finite supply [25,26]. Consequently, Pt is a costly and scarce metal. Thus, reducing its loading or completely replacing it with abundant and cheap materials would be advantageous for lowering the cost of fuel cell vehicles (FCVs) [27]. Gold has received less attention for electrocatalysis than Pt-group metals, mostly because of its subpar catalytic activity. However, in the ORR, bulk gold single-crystal electrodes with orientations of (111), (110), and (100) show promising behavior. As a result, the ORR efficiency of the Au(100) electrode in alkaline media is comparable to that of platinum [28]. To achieve a large specific surface area and lower the cost, gold is frequently dispersed across a nanoparticle form that is adsorbed onto a hard surface [29,30]. Semiconductive oxides are of great interest as support materials because of their strong physicochemical characteristics and excellent stability in alkaline and acidic environments [31]. Additionally, the strong metal–support interaction (SMSI) action, as seen at the Pt/TiO₂ and Au/TiO₂ interfaces [32–35], may help noble metal NPs supported by semiconductive oxides to increase their catalytic activity. Layers of arranged TiO₂ nanotubes laden with Au NPs were recently reported by Macak et al. to exhibit effective oxygen electroreduction in acidic media [36].

According to several studies, metals including Au [37], Cu [38], Co [39], and Ag [40] have been used to functionalize the surfaces of TiO₂ nanoparticles. Noble metal nanoparticles on the exterior of TiO₂ can take up electrons when exposed to radiation, preventing the photon-produced electron-hole pairs from recombining [41,42]. Theoretically, glycerol has an energy density of 6.4 kWh L⁻¹ and is non-flammable, volatile, or toxic. Glycerol is a key by-product of the biodiesel manufacturing process and is sold in large volumes at a discount [43]. Therefore, it is likely that glycerol will be employed in DAFCs as a low-cost, renewable, and eco-friendly fuel [44]. In an alkaline environment, glycerol was electrooxidized in a number of studies [45,46]. Au has been shown to exhibit high reactivity in the heterogeneous catalytic oxidation of glycerol [47–49].

Catalysts made of AuNPs have been used in several chemical reactions. The surface of a gold nanoparticle can be used to minimize the process or selectively oxidize an object. The production of AuNPs for use in fuel cell applications has begun. The auto and display industries may benefit from these developments [50]. Au NPs have a wide range of applications, including drug delivery [51], antibacterial [52], cancer prevention [53], catalytic and antioxidant properties [54], and antiinflammatory and anticancer effects [55]. Additionally, the commercial cost of mastitis in the dairy sector is considerable. It is accompanied by pathological irregularities in the structures of the mammary glands, as well as physical, chemical, and microbiological deviations in milk. Different influences, including host, environment, season, and specific agent parasites, such as *Staphylococcus aureus* and *E. coli*, are responsible for it [56].

Metal and metal oxide nanoparticles (NPs) such as gold, copper, silver, zinc oxide, manganese oxide, and titanium oxide have been identified as the most antibacterial inorganic materials [57]. *S. aureus* and *E. coli* are common pathogenic bacteria that threaten human health [58].

The results of our study focused on the shape and structure of Au NPs based on TiO₂ nanoparticles, along with the electro catalytic activities of Au nanoparticles in acidic, basic, and glycerol-basic solutions. Consequently, the outcomes were compared with those of industrial polycrystalline gold, and our results were excellent compared to industrial polycrystalline. Oxygen–hydrogen gas evolution, surface oxidation, and oxide reduction processes were studied using cyclic voltammetry (CV). For this purpose, Au nanoparticles were positioned on TiO₂-nanoparticles. The observations of TiO₂ NPs and Au NPs/TiO₂ NPs acting satisfactorily as antimicrobial agents against some human pathogenic bacteria are also discussed.

2. Experimental

2.1. Materials

Alfa Aesar Ti foils with a purity of more than 99.5 % and with a thickness of 0.25 mm, tetrachloroauric acid (H[AuCl₄] 99.9+%) as a precursor, 99.0 % isopropanol as a sacrificial donor, perchloric acid HClO₄ 70 % From MERCK, Made in Germany, TiO₂ nanoparticle powder prepared in our lab with a surface area of 109 m²/g, Nafion (5 wt %), H₂SO₄ from Sigma–Aldrich, Potassium chloride GRG KCl (WINLAB), potassium hexacyanoferrate (II) trihydrate K₄[Fe(CN)₆], and flakes extra pure KOH from LOBA Chemie, India. Mueller-

Hinton agar (MHA, HIMEDIA, India), dimethyl sulfoxide (DMSO), potassium hexacyanoferrate(III) $K_3[Fe(CN)_6]$ (MERCK), glycerol, and gentamicin (10 $\mu\text{g/ml}$) were obtained from MERCK.

2.2. Synthesis of TiO_2 nanoparticles powder

Titanium oxide nanoparticle (TiO_2 NPs) powder was created using the anodization procedure. An aqueous solution was used to anodize the Ti foils, containing 0.7 M per chloric acid ($HClO_4$), and Alfa Aesar Ti foils with a purity of more than 99.5 %, utilizing a 2-electrode polypropylene electrochemical cell that operates at room temperature and 20V for an hour with a Ti foil anode and a Pt foil cathode. A centrifuge was used to remove the TiO_2 NPs powder from the solution, and which was then dried overnight at 80 $^\circ\text{C}$. To create the TiO_2 NPs- N_2 powder, the TiO_2 NPs powder was then annealed at 450 $^\circ\text{C}$ under N_2 for 3 h at 5 $^\circ\text{C min}^{-1}$ heating and cooling rate.

2.3. Au photodeposition supported on catalyst supports

The mechanism of Au photodeposition on TiO_2 NPs- N_2 to produce Au NPs/ TiO_2 NPs- N_2 catalyst using UV-400 W is shown in Fig. 1. Radiation with UV-400 W is suitable for Au to be reduced and deposited onto the surface of TiO_2 NPs- N_2 powder [59,60]. The anion $[AuCl_4]^-$ is converted to Au metal nanoparticles by the photoelectrons generated by TiO_2 nanoparticles. As opposed to this, aldehyde is produced when isopropanol and photogenerated holes from the band of valence interact [59–63]. In contrast, UV irradiation leads to the reduction and fixation of Au NPs on the exterior of the TiO_2 NPs- N_2 powder.

2.3.1. Synthesis of Au nanoparticle on TiO_2 nanoparticles support

150 mg The catalyst support TiO_2 NPs - N_2 was mixed with 10 mM $H[AuCl_4]$ and 0.3 M isopropanol in a glass beaker and then irradiated using a UV lamp (400 W) for 2h under magnetic stirring. The intensity or power used during the experiments was measured using a Thorlab instrument at a wavelength of 380 nm and power of 39 mW. During the irradiation of the solution, in the case of Au photodeposition on TiO_2 NPs- N_2 , it was obvious that the yellow color turned white, indicating the adsorption of gold on the exterior of the TiO_2 NPs- N_2 powder.

Centrifuging The solution was centrifuged to separate of the Au NPs/ TiO_2 NPs- N_2 powder, which was subsequently collected, cleaned with deionized water, then overnight drying at 80 $^\circ\text{C}$. TiO_2 NPs- N_2 powder with loaded Au was used to prepare ink by weighing 50 mg of Au NPs/ TiO_2 NPs - N_2 powder and adding 1 ml DI (deionized) water plus 10 μL of 0.5 wt % Nafion as a binder and then homogenized by using an ultrasonic bath to prepare the ink for the electrochemical experiments.

A typical three-electrode cell was used to conduct electrochemical measurements with a solution of 2 M KOH, 1 M H_2SO_4 , and 2 M KOH +0.1 M glycerol, A typical three-electrode cell was carried out to conduct the electrochemical measurements. A platinum foil counter electrode was used. The operating electrode was a polycrystalline platinum electrode with an area of 0.07 cm^2 . A Luggin capillary linked the saturated calomel electrode (SCE), which served as the reference electrode, to the cell. A micropipette was used to load the electrocatalyst (Au NPs/ TiO_2 NPs- N_2) onto the electrode surface. The reaction scheme is shown schematically in Fig. 2.

2.4. Transmission electron microscopy (TEM)

Transmission electron microscope (JEOL JEM-2100F) set to 200 kV, the TEM pictures were captured.

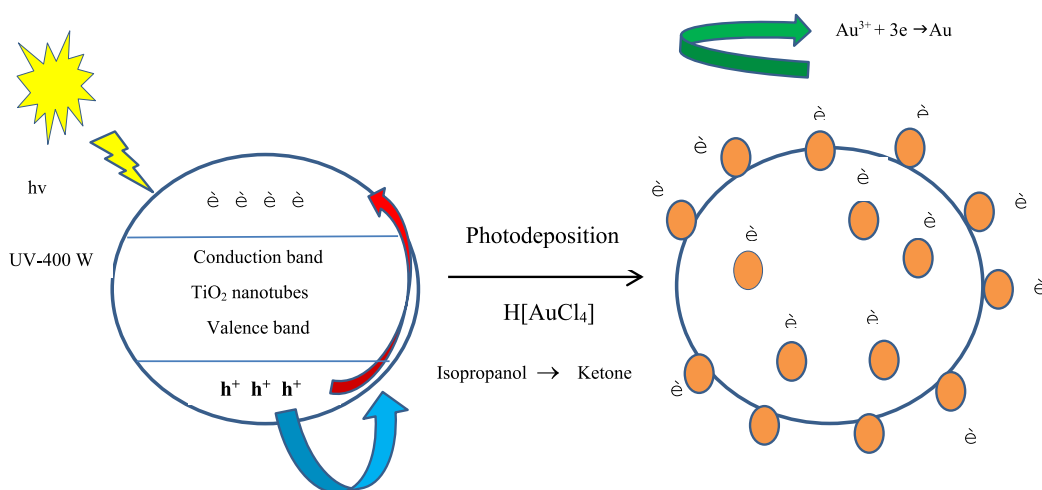


Fig. 1. Mechanism of Au photodeposition to prepare Au NPs/ TiO_2 NPs- N_2 catalyst using UV-400 W lamp.

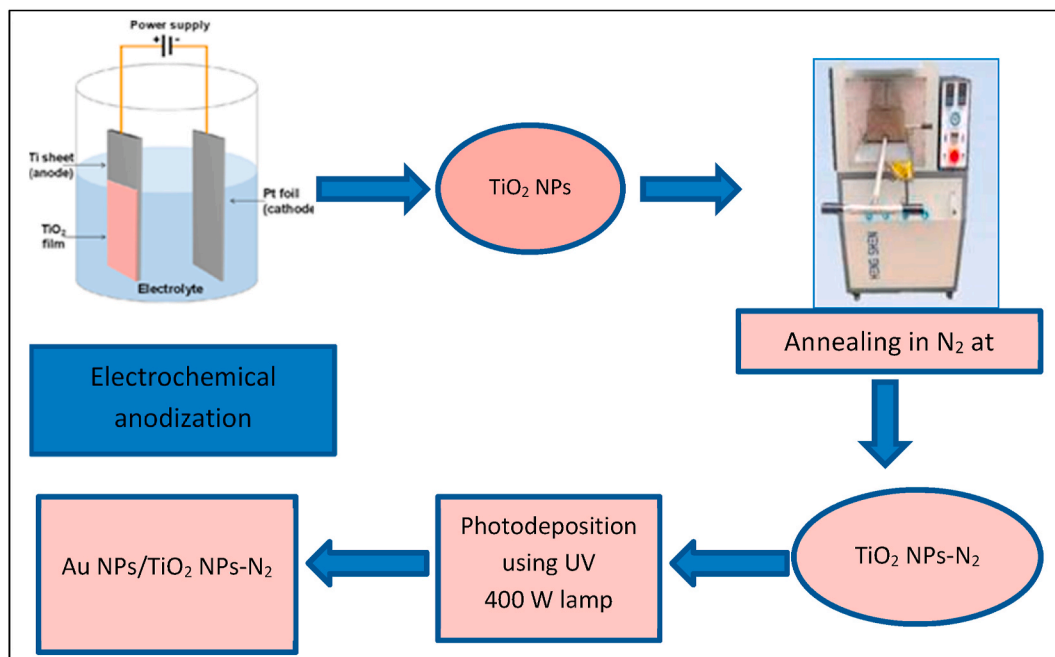


Fig. 2. The schematic diagram for the preparation of Au NPs/TiO₂ NPs-N₂.

2.5. Electrochemical investigations

Cyclic voltammetry (CV) was performed using a standard 3-electrode Pyrex glass cell and programmable galvanostat/potentiostat (Autolab, FRA2, AUTOLAB, TYPE III). The reference electrode was pure Pt foil, while the auxiliary electrode was SCE. The SCE electrode was the sole electrode used to calculate the potential presented in the written content. A saturated calomel reference electrode (SCE) and a Pt wire auxiliary electrode were utilized. In addition, a working electrode made of 3 mm polycrystalline Pt with a surface area of 0.07 cm² was employed. Cyclic voltammetry signals were obtained using the NOVA 1.9 software. By ultrasonically blending 50 mg of the catalyst with 1 mL of deionized water for 30 min, a consistently distributed suspension ink (i.e., homogenized ink) was produced. Therefore, a Pt polycrystalline working electrode with a 3 mm diameter and 0.07 cm² thickness was covered with 3 L of the suspension product. 1 L of Nafion (5 wt percent) solution was applied to the catalyst surface after it had dried at 40 °C, and extra drying time was permitted. Consequently, the operating electrode was fabricated, and the specific metal loading at the Pt operating electrode surface was approximately 0.020 mg (20.0 g) in 3 L of Au NPs/TiO₂ NPs-N₂. In 2 M KOH, 1 M H₂SO₄, and 2 M KOH +0.1 M glycerol, electrochemical measurements were conducted.

2.6. Material characterization

With the aid of an inductively coupled plasma spectroscopy equipment, the Au weight loading in the produced components of interest was ascertained. For this assessment, the components were dissolved in an acidic solution of aqua regia (3HCl:1HNO₃) using a Teflon tube vessel system and a high-pressure microwave digestion system (MARSX; CEM) operating at 450 K and 170 psi. A Microwave Accelerated Reaction System (MARS) was employed for the digestion procedure.

2.7. TiO₂ nanoparticles' antimicrobial properties

The disc diffusion technique was used to gauge the TiO₂ NPs' antimicrobial properties. The experiment was run against reference strains of gram-positive (*S. aureus*) and gram-negative (*E. coli*) bacteria from the AL-Garfi Laboratory in Thamar, Yemen. Mueller-Hinton Agar (MHA) was inoculated at 105 cells/mL. Briefly, 20 mL of MHA was placed on Petri plates and left to set. Petri dishes were then properly positioned with 6 mm thick sterile discs. Finally, each disc was filled with TiO₂ NPs at various doses (1, 2, 4, 8, and 16 mg/mL). The reference standard (10 µg/mL) used was gentamicin (GM) disc, and the negative control (DMSO) was employed. All of the plates had an incubation period of 37 °C [64,65].

2.8. Antimicrobial activity of Au NPs/TiO₂ nanoparticles

A typical disc diffusion technique was utilized for antibacterial experiments with gram-positive *Staphylococcus aureus* and gram-negative *Escherichia coli* [66]. Sterile paper discs measuring 6 mm in diameter were placed on swabbed MHA plates. Various

concentrations of nanoparticles (1, 2, 4, 8, and 16 mg/ml) were poured over the discs. Additionally, a conventional antibiotic disc (gentamicin 10 $\mu\text{g/ml}$) was positioned alongside dimethyl sulfoxide (DMSO) as a checkpoint. for 24 h, at 37 $^{\circ}\text{C}$, the plates were cultured. Three plates were used for each sample. An inhibitory zone is also detected. mm after the incubation (mm).

3. Results and discussion

3.1. Size and morphology

Our most recent research, which was previously published [67], contained a typical TEM image and XRD pattern of TiO_2 NPs- N_2 and Au NPs/ TiO_2 NPs- N_2 are given in Fig. 3. It was demonstrated that most of the TiO_2 NPs- N_2 were circular. According to the TEM image [67], the average nanoparticle size of annealed TiO_2 in nitrogen was 12.01 ± 2.39 nm. The TEM images demonstrate the size of the gold nanoparticles and that the Au NPs/ TiO_2 NPs- N_2 powder catalyst was formed without changing the original shape of the TiO_2 nanoparticles. The images demonstrate that the majority of Au-NPs are evenly distributed over a TiO_2 nanoparticle support that has been annealed in N_2 , confirming that most Au NPs/ TiO_2 NPs- N_2 are round. The mean size of the Au Nanoparticles in the TEM image is $(23.18 \pm 4.39$ nm) Fig. 3c, which is almost twice as large as that of TiO_2 -NPs.

Equation (1) was employed to ascertain the average number of gold atoms present in each nanoparticle. A spherical form was used to compute the average number of Au atoms that exist in each nanoparticle. This estimate was calculated using Equation (1).

$$N = \pi \rho N_A D^3 / 6 M \quad (1)$$

where M is 197 g/mol, which is the atomic mass of gold (Au), D is the average diameter of nanoparticles in nanometers, N_A is

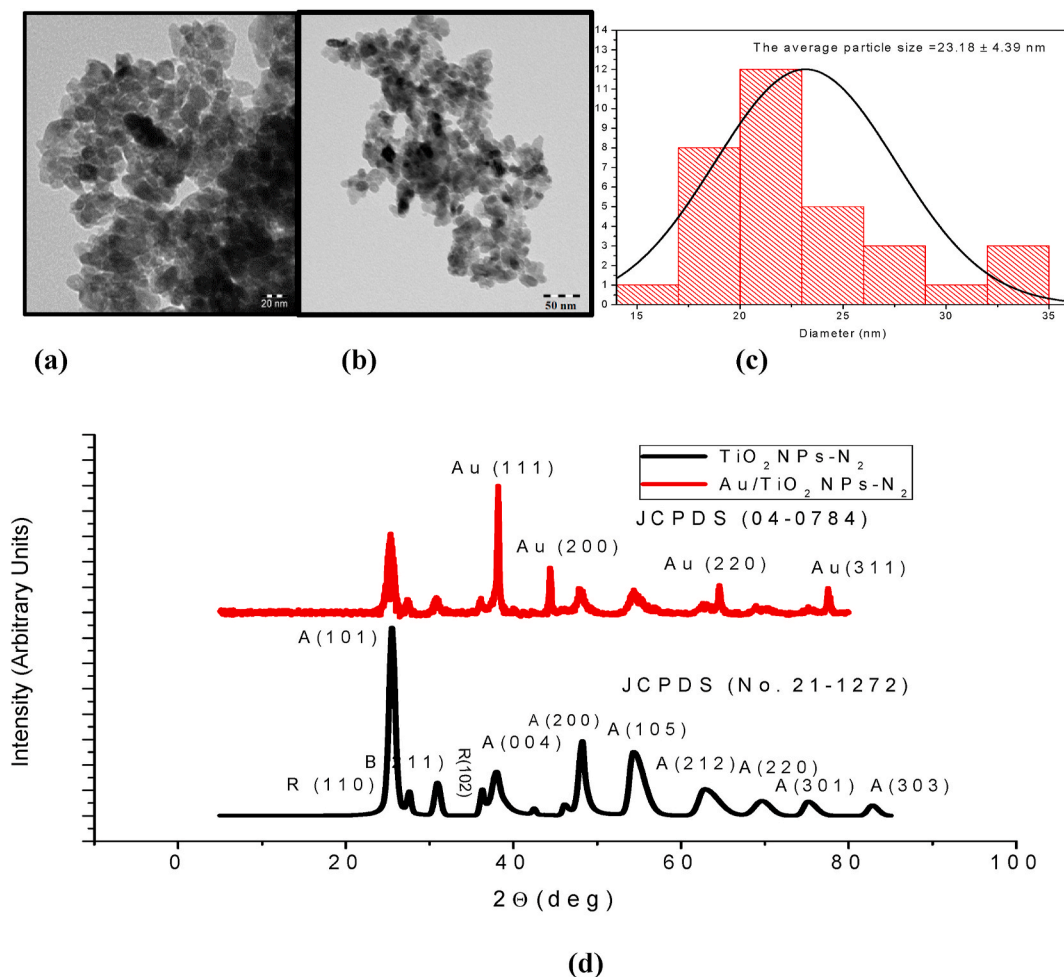


Fig. 3. TEM images of Au NPs/ TiO_2 NPs- N_2 powder (a) at 20 nm and (b) at 50 nm and (c) corresponding particle size distribution histograms of Au NPs/ TiO_2 NPs- N_2 catalyst. (d) XRD pattern of TiO_2 NPs- N_2 and Au nanoparticles supported on TiO_2 nanoparticles annealed in ambient of nitrogen. After Jamil et al. [67].

Avogadro's number of element atoms ($6.02214179 \times 10^{23}$), and ρ is the gold density (1.93×10^{-20} g/nm³) [68].

In XRD the (JCPDS anatase cards TiO₂ (No. 21–1272)) card for TiO₂ and the (JCPDS 04–0784) card for Au NPs.

3.2. Electrochemical investigations of Au NP/TiO₂ NPs-N₂ catalyst

3.2.1. Cyclic voltammetry in ferrocyanide system

Fig. 4 shows the CV profile of 10 mM K₄[Fe(CN)₆], K₃[Fe(CN)₆] and 0.5 M KCl on Au NPs/TiO₂ NPs-N₂ and the polycrystalline working electrodes of Au and Pt. For the Au polycrystalline operating electrode, the peak-to-peak separation (ΔE_p) for the 10 mM Potassium Ferro cyanide/ferric cyanide complex (10 mM [Fe(CN)₆]^{3-/4-}) for the Au polycrystalline working electrode was 70 mV at 50 mV/s, which is approximately equivalent to the hypothetical quantity of 59/n mV with n = 1. The proportion of backward and forward peak currents (I_{pa}/I_{pc}) was 0.98. The collected findings demonstrated that the Fe (III)/Fe (II) approximate reversible mechanism was used to generate the typical electrochemical behavior of Au NPs in potassium ferricyanide solution [69]. Au NPs were used to modify the TiO₂ NPs-N₂ electrode, and the results showed a noticeable drop in the current and an increase in (ΔE_p). The reversibility of the couple is lost as a result of the impact of the nanoparticles on the electronic transmission, which makes it more challenging. Table 1 shows that the ratio (I_{pa}/I_{pc}) remained constant, that is, an equal quantity of redox mediator was both reduced and oxidized. The (ΔE_p) decreases in the following order: Au polycrystalline electrode, Au NPs/TiO₂ NPs-N₂, and Pt polycrystalline electrodes, as shown in the table. The pattern of the order was the same as that of the active surface area, as shown in Table 1. Therefore, the Au WE has the largest active surface area and the most heterogeneous film. The smallest ΔE_p value indicates a high electrical conductivity.

The photo-deposited Au NPs/TiO₂ NPs-N₂ electrodes exhibit typical Nernstian behavior, as shown in Fig. 4. The values of the pertinent parameters $E^0 = 249$ mV, $\Delta E_p = 76$ mV, and $I_{ap}/I_{cp} = 1.02$ (n = 1) amply demonstrate the reproducibility and similarity of the electrode response to those of produced gold electrodes.

The I_p/I_b values for the Au NPs/TiO₂ NPs-N₂ and for 0.07 cm² gold and platinum polycrystalline working electrodes for each of the anodic and cathodic pathways, the peak height-mA/cm², are shown in Table 1 together with the I_p (peak height-mA/cm²) values.

In some previous studies, the electrocatalyst Au NPs/nano-diamond (ND)/carbon ionic liquid electrode (CILE) was characterized electrochemically by cyclic voltammetry in Ferro cyanide system with peak anode current (I_{pa}) of 64.18 μ A, peak cathode current (I_{pc}) was found to be (66.53 μ A) and the ratio I_{pa}/I_{pc} equals to 0.964 [70]. In our research, the electrochemical characteristics of the Ferro cyanide system electrocatalyst Au NPs/TiO₂ NPs-N₂, with a peak anode current (I_{pa}) equal to (2.751 mA/cm²), peak cathode current (I_{pc}) equal to (-2.708 mA/cm²) and the ratio I_{pa}/I_{pc} is 1.02, that is, with a higher current.

Table 2 summarizes the oxidation and reduction peaks of potentials, separation, and ΔG^0 (kJ) of Au NPs/TiO₂ NPs-N₂, 0.07 cm² Au and Pt polycrystalline working electrodes in a ferrocyanide system.

Fig. 4 illustrates the use of [Fe(CN)₆]^{3-/4-} redox probes in the CV method to examine the electron transport properties of various electrode surfaces. Compared to the bare Pt polycrystalline electrode, Au NPs/TiO₂ NPs-N₂ exhibited higher [Fe(CN)₆]^{3-/4-} redox currents. Because of the effective ability of TiO₂ NPs-N₂, the potential difference between the oxidation and reduction peaks of the [Fe(CN)₆]^{3-/4-} redox probe. When redox probes were placed on Au NPs/TiO₂ NPs-N₂, their redox currents were further increased compared to when they were placed on bare Pt polycrystalline electrodes, proving that the Au NPs significantly increased electron transfer capabilities [71].

The Au NPs/TiO₂ NPs-N₂ samples were evaluated as electrodes using a one-electron redox couple to ensure that there was an extremely strong electrical link between Au and the Ti electrode underneath it. The voltammogram curves for the reduction of K₃Fe(CN)₆ are shown in Fig. 4 for electrodes made of Au NPs/TiO₂ NPs-N₂, Au polycrystalline electrodes with an area of 0.07 cm², and Pt polycrystalline electrodes with an area of 0.07 cm². The predicted reversible action for the reduction of the Pt polycrystalline electrode is shown in the voltammogram of the Au NPs/TiO₂ NPs-N₂ electrodes. This implies that titanium and electrodeposited gold sheets have acceptable adhesion and electrical contact.

The surface area of the Au NPs/TiO₂ NPs-N₂ electrode was calculated using 10 mM K₄Fe(CN)₆ in 0.5 M KCl by obtaining cyclic voltammograms. This was performed with the aim of electrochemically determining the actual surface of the electrode and comparing

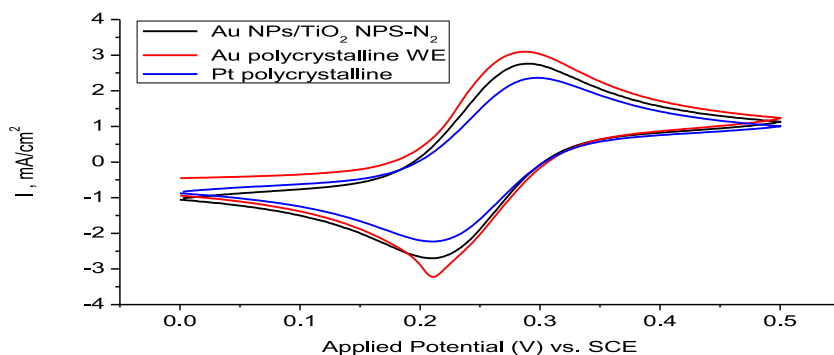


Fig. 4. CVs of 10 mM K₄[Fe(CN)₆], K₃[Fe(CN)₆] and 0.5 M KCl, scan rate 50 mV/s, contains Au NPs/TiO₂ NPs-N₂ powder, in contrast with Au polycrystalline and Pt polycrystalline electrodes with area 0.07 cm², window of potential range 0–0.5V.

Table 1Comparison between Au NPs/TiO₂ NPs-N₂ powder, 0.07 cm² Au and Pt polycrystalline working electrodes in Ferro cyanide system.

Electrode	I _{pa} (mA/cm ²)	I _{pc} (mA/cm ²)	I _{pa} /I _{pc}
Au NPs/TiO ₂ NPs-N ₂	2.751	-2.708	1.02
Au polycrystalline electrode	3.172	-3.233	0.981
Pt polycrystalline	2.408	-2.209	1.09
Au NPs/nano-diamond (ND)/carbon ionic liquid electrode (CILE)	64.18 μA	66.53 μA	0.964 [70]

Table 2Oxidation and reduction peaks of potentials, reduction/oxidation peaks separation and also ΔG°(kJ) of Au NPs/TiO₂ NPs-N₂, 0.07 cm² Au and Pt polycrystalline working electrodes in ferrocyanide system.

Electrode	E _{pa} (V)	E _{pc} (V)	ΔE (V)	ΔE(mV)	E° (V)	ΔG° (kJ)
Au NPs/TiO ₂ NPs-N ₂	0.287	0.211	0.076	76	0.249	24.03
Au polycrystalline electrode with area 0.07 cm ²	0.284	0.211	0.073	73	0.248	23.93
Pt polycrystalline electrode with area 0.07 cm ²	0.290	0.210	0.08	80	0.25	24.12

the fabricated electrodes with a pure gold electrode. The surface area of the electrode was established by assuming the Randles-Sevcik Equations (2) and (3) [72–74] from the peak current measured by cyclic voltammetry and the diffusion coefficient of hexacyanoferrate:

$$i_{pa} = (2.69 \times 10^5) n^{3/2} A D_o^{1/2} v^{1/2} C_o \quad (2)$$

$$A = i_{pa} / (2.69 \times 10^5) n^{3/2} D_o^{1/2} v^{1/2} C_o \quad (3)$$

where I_{pa} stands for the anode's peak current in mA, n is the number of electrons transferred (1), A is the electrode surface area, D_o is the diffusion coefficient (9.382 10⁻⁶ cm² s⁻¹), v is the scan rate (50 mV/s), and C_o is the number of electroactive species in moles/cm³ (0.5 M KCl) in moles. The surface area (geometric area) of the three electrodes calculated using the Randles-Sevcik relation was approximately close to the surface area of the three electrodes, which was found practically (0.07 cm²).

3.2.2. Cyclic voltammetry in 2 M KOH system

Cyclic voltammograms were obtained using commercial Au disks (Au working electrodes) and Au NPs/TiO₂ NPs-N₂ electrodes in an alkaline supporting electrolyte. The results are shown in Fig. 5. When measured in 2.0 M KOH under N₂ saturation, the voltammograms of the Au disk electrode and Au NPs/TiO₂ NPs-N₂ showed three areas based on the applied potential (Fig. 5). The regions in Fig. 5 are: (I) is the oxidation peak of the Au catalyst, (II) is the oxygen evolution, (III) is the reduction peak of the Au catalyst, and (IV) is the oxygen reduction. At higher potentials, space (IV) reveals the adsorption of oxygenated species (oxidation peaks) and desorption (reduction peaks) at the electrode surface. Small currents related to both the double-layer capacity charge and discharge are typical of double-layer space. (V), where no net electrochemical reaction occurred [75,76].

When the gold nanoelectrode was cycled through a solution of alkali (Fig. 5), there were two oxidation processes and one reduction process. The creation of the oxide layer Au–O and the anodic peaks at 0.2 and 0.6 V are often ascribed to each other [77,78]. Au–O is subsequently decreased at -0.02 V during the cathodic scan [78]. In both acidic and alkaline liquids, the polycrystalline commercial electrodes exhibit qualitatively identical curves. The last cycle of a CV scan in 2.0 M KOH from (-0.8-0.7 V) at 50 mV/s was used to

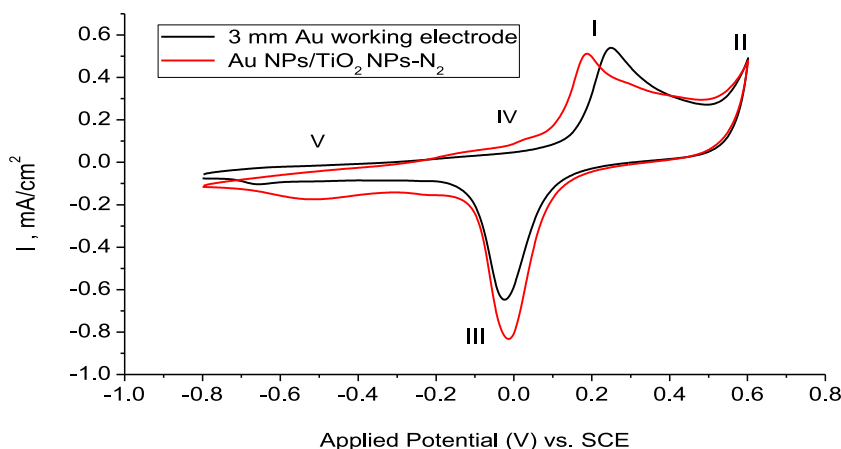


Fig. 5. CV of 3 mm Au working electrode, Au NPs/TiO₂ NPs-N₂ powder all in 2 M KOH purged in saturated N₂ for 3 min at a scan rate of 50 mV/s.

determine the electrochemical active surface area (ECSA-ECSA) of the Au NPs-TiO₂ NPs-N₂ catalyst as it had been manufactured. A monolayer of Au oxide was formed and reduced, as shown by the anodic peak of the forward scan and the cathodic peak of the reverse scan [79]. According to measurements made from the reduction peaks at -0.0114 V and -0.0237 V, respectively, with 0.386 mC cm^{-2} of charge density and a double layer correction, the ECSA of the Au NPs-TiO₂ NPs-N₂ catalyst is $19.05 \text{ cm}^2 \text{ mg}^{-1}$, and for the Au polycrystalline working electrode, it is $15.90 \text{ cm}^2 \text{ mg}^{-1}$ [79]. Equations (4) and (5) were used to determine the electrochemical active surface area (ECSA-ECSA) of the Au NPs-TiO₂ NPs-N₂ catalyst in 2 M KOH, as previously reported [80].

$$Q_h = \frac{\text{Peak area (mA.V)}}{\text{Scan rate} \left(\frac{\text{V}}{\text{s}} \right)} \quad (4)$$

$$\text{ECSA} = Q_h \text{ in mC} / q \text{ (constant in mC/cm}^2\text{)} \quad (5)$$

3.2.3. Cyclic voltammetry in 1 M H₂SO₄ system

An overlap between the oxidation peaks of the Au working electrode and the Au NPs-TiO₂ NPs-N₂ powder was observed; therefore, the Au catalyst could not be loaded on the Au working electrode.

In Fig. 6, peak (a) is the anodic oxidation peak of the gold polycrystalline working electrode and Au NPs-TiO₂ NPs-N₂ powder crystalline, peak (b) is oxygen evolution, (c) is the cathodic reduction peak of the gold surface oxide and Au NPs-TiO₂ NPs-N₂ powder crystalline, peak (d) is the desorption of chloride traces that result from H[AuCl₄] and peak (e) is the adsorption of chloride traces that result from H[AuCl₄].

The cathodic peak (c) in Fig. 6 (A) is due to the reduction of the gold surface oxide, whereas the anodic peak (a) is related to the oxidation of gold. Peak (b) corresponds to oxygen evolution, peak (d) to oxygen reduction, and peak (f) to hydrogen evolution. The adsorption of protons occurs in area (d), where the peak (d) is located. Fig. 6 (A) shows a cyclic voltammogram of a working electrode made of 3 mm polycrystalline Au in the potential range of 0–1.5 V set at a scan rate of 50 mV/s. The oxidative peaks a and b are related to the evolution of oxygen and oxidation of precipitated gold to Au(III), respectively. The reduction of gold surface oxide (at 0.88 V), reduction of protons, and hydrogen development, respectively, are attributed to the reductive peaks c, d, and e [81–83]. The reduction peak in the second cycle, as shown in Fig. 6, moved to a higher positive potential, facilitating the electrodeposition of gold on the gold nuclei that had already been deposited [84]. Golden-colored deposits can be seen by cycling the potential from an initial 0–1.5 V, notably at higher concentrations of gold deposition solutions and longer deposition durations. More gold was placed onto the substrate during a longer deposition period, although some electrodeposited particles were not spherical, which may have led to the formation of aggregates. Fig. 5 illustrates how the activation/stabilization cyclic voltammetry scans of nano-sized metal electrodes on a Pt polycrystalline electrode reveal the widely recognized gold behavior when used in an extremely acidic solution [85]. The layer was lowered within the cathodic sweep at a potential of approximately 0.896 V. The development of a thin oxide layer on the outside of gold drives the oxidation reaction at a high voltage (1.3 V). After 15 cycles, no appreciable variations are observed between the two subsequent scans.

The last cycle of a CV scan in 1.0 M H₂SO₄ from 0 to 1.6 V at 50 mV/s was used to find the electrochemical active surface area (ECSA-ECSA) of the Au NPs-TiO₂ NPs-N₂ catalyst as it had been manufactured. A monolayer of Au oxide is formed and reduced as evidenced by the anodic and cathodic peaks on the forward and backward scans, respectively, with 0.386 mC cm^{-2} charge density and a double layer correction, the ECSA of the Au NPs-TiO₂ NPs-N₂ catalyst was determined to be $14.0 \text{ cm}^2 \text{ mg}^{-1}$ from the reduction peak at 0.89 V. Based on the cyclic voltammograms generated, the total charge of the hydrogen desorption area (Q_H) with the adjustment of the double layer region as stated in Eq. (6) could be used to compute the real surface area (A_r) was calculated using Eq. (7) or electrochemical active surface area (EASA-ECSA) by using Eq. (8) of the Au NPs-TiO₂ NPs-N₂ electrode. During the experiment, we considered that monolayer hydrogen desorption on smooth Au corresponds to a theoretical charge of 0.386 mC cm^{-2} (Q_m) [86].

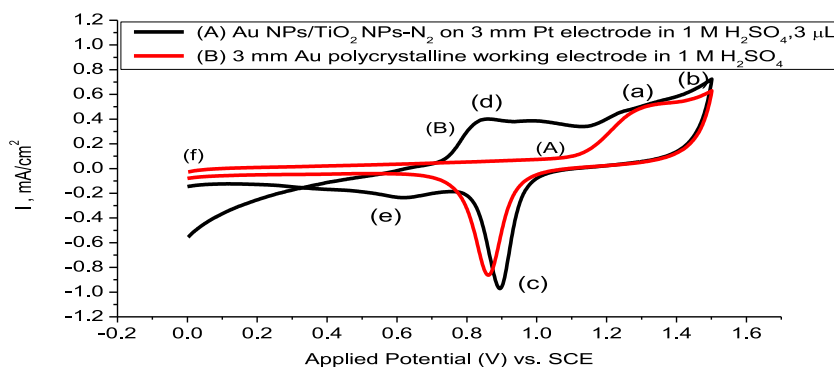


Fig. 6. CV of (A) Au polycrystalline working electrode and (B) photodeposition of 3 μL of crystalline Au NPs-TiO₂ NPs-N₂ powder was placed onto a working electrode of 3 mm Pt polycrystalline, all in 1 M H₂SO₄ at a scan rate of 50 mV/s.

$$Q_H = \frac{1}{V_b} \int_{E_1}^{E_2} I \cdot dE \quad (6)$$

where V_b is the scan rate mVs^{-1} , dE is the potential (mV), and I is the current density mA mAcm^{-2} . Thus, the following formulae can be used to obtain the actual surface area (A_r) and roughness factor (R_f) of the final electrode:

$$A_r (\text{EASA-ECSA}) = Q_H/Q_m \quad (7)$$

$$R_f/A_r (\text{EASA-ECSA})/A_g \quad (8)$$

where A_g is equal to 0.07 cm^2 in terms of the geometric area of the constructed electrode. The standard practice is to assess the performance of electrocatalysts using their electrochemically active surface area (EASA-ECSA). The roughness factor is directly proportional to the electrochemically active surface area; that is, an increase in the roughness factor indicates an increase in the electrochemically active surface area. According to the reduction peak charge and ICP analysis measurements of the mass loading, electrochemically active surface area, and roughness factors (R_f) of the Au NPs catalysts, Table 3 provides these data. However, the Au NPs-TiO₂ NPs-N₂ showed a lower roughness factor than that of the Au polycrystalline working electrode, as shown in Table 3.

The electrochemical active surface area (EASA-ECSA) of Au polycrystalline electrode was found to be 0.29 cm^2 , while the Au NPs/TiO₂ NPs-N₂ electrode offered a lesser electrochemical active surface area of 0.28 cm^2 .

Au NPs-TiO₂ NPs-N₂ powder electrode can be used as a chloride sensor in an acidic solution (1 M H₂SO₄). In Fig. 7, we note that desorption and adsorption of chloride take place on TiO₂ NPs-N₂ powder during the photodeposition of H[AuCl₄]. In the cyclic voltammetry of Au NPs-TiO₂ NPs-N₂ in an acidic medium (1 M H₂SO₄), chloride peaks appear, that is, desorption of chloride traces that result from [AuCl₄]⁻ (d) and adsorption of chloride traces that result from H[AuCl₄] (e). To remove these peaks, the Au NPs-TiO₂ NPs-N₂ must be treated with 0.1 M NaOH, that is, the powder of Au NPs-TiO₂ NPs-N₂ with 0.1 M NaOH to remove chloride, where OH⁻ replaces Cl⁻ as in equation (9).



With 50 mV/s in 1 M HClO₄ with a potential range of -500 to 1700 mV, the cyclic voltammograms of the Au polycrystalline working electrode and Au NPs-TiO₂ NPs-N₂ powder electrodes are shown in Fig. 8. A typical voltammogram demonstrating a spotless gold surface is shown in Fig. 8.

The cyclic voltammogram of 10 μL saturated KCl on a 3 mm Au electrode was obtained in 1 M HClO₄ at 50 mV/s and a potential range between 0 and 1500 mV, as shown in Fig. 9, where peak (a) is the desorption of chloride and peak (b) is the adsorption of chloride.

3.2.4. Glycerol oxidation reaction of gold supported on TiO₂ NPs-N₂

Investigated was the electrocatalytic oxidation of glycerol in 2.0 M KOH and 0.1 M glycerol on Au NPs/TiO₂ NPs-N₂. As shown in Fig. 10, the glycerol oxidation CV curves have two distinct anodic peaks in both the forward and backward scans, which is indicative of an alcohol electrooxidation process [87]. Fig. 10 illustrates the electrocatalytic activity for the glycerol oxidation reaction, that is, the CVs of the 3 μL Au NPs/TiO₂ NPs-N₂ powder catalyst and the Au polycrystalline electrode in 2 M KOH and 0.1 M glycerol. The peak current density for the Au NPs/TiO₂ NPs-N₂ powder catalyst is shown in Fig. 10 for the 0.1 M glycerol concentration in an alkaline environment, and it was found to be 57 mA/cm^2 when scanning forward scan and 40.9 mA/cm^2 in the backward scan. The Au NPs/TiO₂ NPs-N₂ powder showed excellent catalytic activity for glycerol electrooxidation.

Alcohol with lower pK_a is more reactive. Because glycerol has a lower pK_a than ethylene glycol (EG) (14.77) and methanol (15.50) under high pH conditions, glycerol deprotonates more easily into glycerolate with high reactivity, which results in large total electrooxidation activity. Glycerol is projected to be a promising fuel for AEM-DGFCs (glycerol fuel cells with an anion-exchange membrane) using Au anode catalysts. Electrooxidation of glycerol was carried out using Au NPs/TiO₂ NPs-N₂ with an average diameter of 26.8 nm. In 2 M KOH with 0.1 M glycerol, a cyclic voltammogram of Au NPs/TiO₂ NPs-N₂ is displayed in Fig. 10. The cyclic voltammograms demonstrated the low activity of the Au NPs/TiO₂ NPs-N₂ electrode in 2 M KOH. The complete oxidation of glycerol in alkaline environments occurs, hypothetically speaking, as follows, according to Jeffery and Camara [88]:



The electro-oxidation of glycerol to its intermediates was attributed to the anodic peak (a) in the forward-going positive scan, and the oxidation of intermediate species or residues that were still present in the forward-going positive scan belonged to the anodic peak

Table 3

Electrochemically active surface area (ECSA) and roughness factors (R_f) of Au polycrystalline working electrode and Au NPs/TiO₂ NPs-N₂ powder in 1 M H₂SO₄.

Catalysts	Q_H (charge density), mC	Surface area (cm^2) (ECSA)	R_f	Mass loading (g/m^2)
Au polycrystalline working electrode	0.113	0.29	4.1	–
Au NPs/TiO ₂ NPs-N ₂ powder	0.108	0.28	4.0	2.86×10^{-4}

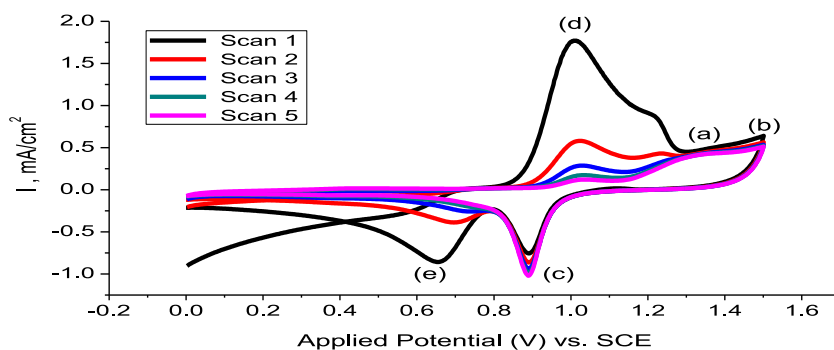


Fig. 7. CV for the photodeposition of Au NPs-TiO₂ NPs-N₂ powder on a 3 mm Au working electrode in 1 M H₂SO₄ at a scan rate of 50 mV/s (effect of scan).

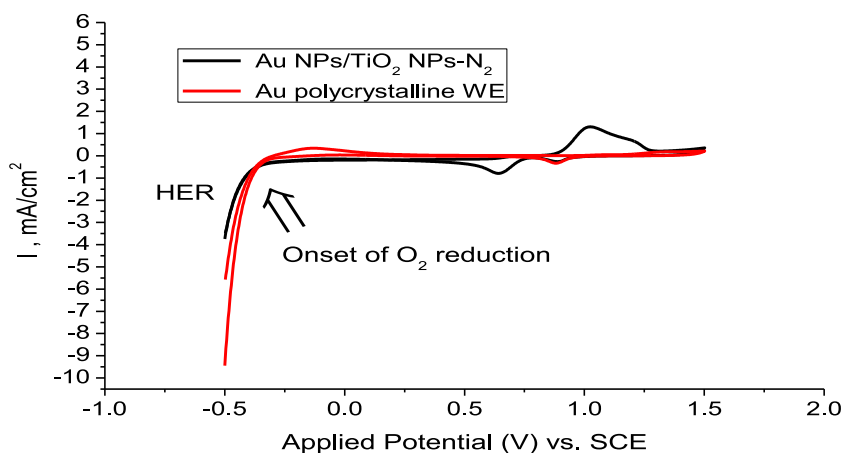


Fig. 8. CV for Au polycrystalline working electrode and photodeposition of Au NPs/TiO₂ NPs-N₂ powder 10 μ L placed onto a working 3 mm Pt electrode all in 1 M HClO₄ at a 50 mV/s scan rate (potential range from -0.5 - 1.5 V).

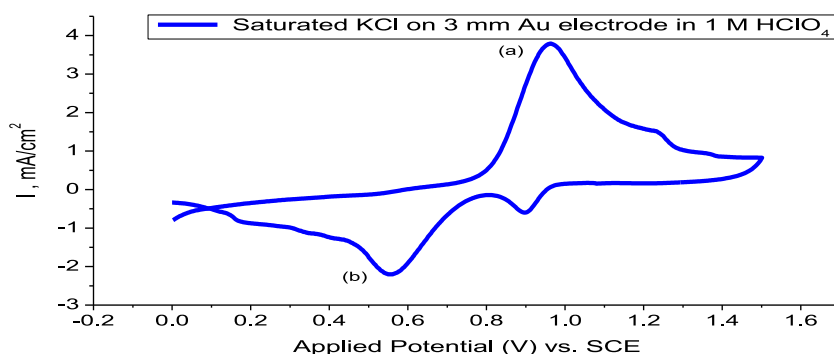


Fig. 9. Saturated KCl on 3 mm Au electrode in 1 M HClO₄ at scan rate was 50 mVs⁻¹, 10 μ L.

(b) in the backward-going negative scan. The heights of the forward (I_f) and backward (I_b) anodic peak currents are affected by factors such as temperature, scan rate, quantity of metal nanoparticles loaded on the electrode surface, concentration of the supporting electrolyte, and (for I_b) species formed on the surface of the metal nanoparticles [89].

As shown in Table 4, the I_f/I_b ratio for the gold working electrode (1.35) in the GOR was lower than that of the Au NPs/TiO₂ NPs-N₂ powder (1.39) in the GOR, indicating different electrodes. It is also noted that the I_b/I_f ratio for the Au working electrode (0.74) in the GOR is higher than that of the Au NPs/TiO₂ NPs-N₂ powder (0.72) in the GOR, which is due to the two different electrodes.

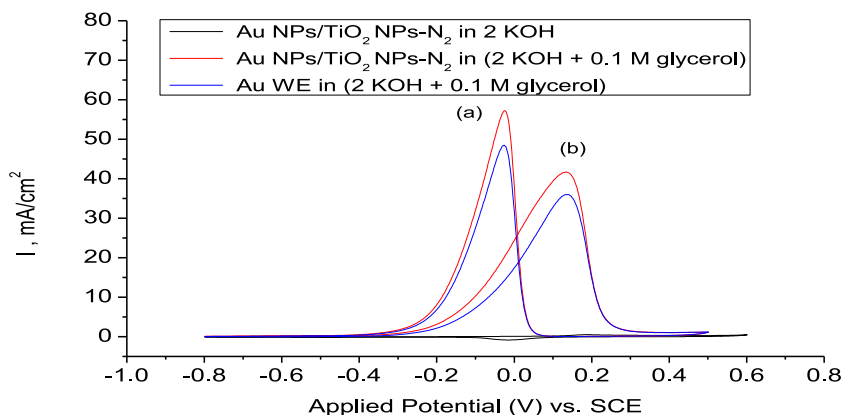


Fig. 10. CV of 3 mm Au working electrode, Au NPs/TiO₂ NPs-N₂ powder in (2 M KOH+ 0.1 glycerol) at a scan rate of 50 mV/s.

Table 4

The values of I_f, I_b, I_f/I_b and I_b/I_f of Au working electrode and Au NPs/TiO₂ NPs-N₂ for glycerol oxidation reaction (GOR).

Catalysts	I _f (mA/cm ²)	I _b (mA/cm ²)	I _f /I _b	I _b /I _f
Au working electrode	48	35.5	1.35	0.74
Au NPs/TiO ₂ NPs-N ₂	57	40.9	1.39	0.72

3.3. The antimicrobial effect

3.3.1. The antibacterial effect of the TiO₂ NPs

The antibacterial activities of TiO₂ NPs (TiO₂ nanoparticles) versus *E. coli* and *S. aureus* are shown in Fig. 11. TiO₂ nanoparticle concentrations of 1, 2, 4, 8, and 16 mg/ml are represented by 1, 2, 3, 4, and 5, respectively, while DMSO served as a negative control and gentamicin (10 µg/ml) served as a standard reference (positive control) in numbers 6 and 7. The disc diffusion technique (DDM) [90] was used to assess the antibacterial activity of TiO₂ NPs (TiO₂ nanoparticles) versus *E. coli* and *S. aureus*. Fig. 11 displays the outcomes. These findings demonstrate that whereas TiO₂ NPs had less effect on *E. coli*, they may have had inhibitory effects on *S. aureus*. TiO₂ NPs also exhibited greater inhibition, even at reduced doses (Table 5) and Fig. 12. The MIC of TiO₂ NPs was determined against all selected bacteria (Table 6).

3.3.2. The Au NPs/TiO₂ NPs antimicrobial effect

The use of Au NPs (nanospheres) with a diameter of 20–37 nm for anticancer and antibacterial actions is possible [91]. The antimicrobial activity of the Au NPs/TiO₂ NPs was assessed using the disc diffusion technique. Strong antibacterial properties were observed for both the gold ions and Au NPs. Gram-positive and gram-negative bacteria were inhibited by solutions containing gold NPs, as shown by their antibacterial activity at various concentrations. Human pathogenic microorganisms of both gram-positive and gram-negative bacteria, such as *S. aureus* and *E. coli*, are susceptible to the antibacterial effects of AuNPs. The permeability and respiratory functions of the bacterial cell membrane were disturbed by the addition of Au NPs at concentrations of 1, 2, 4, 8, and 16 mg, as shown in Fig. 13., which shows the results of the antimicrobial assay. These results demonstrated that the Au NPs had larger inhibition zones. For Gram-positive *Staphylococcus aureus* at doses of 1, 2, 4, 8, and 16 mg/ml of synthetic Au NPs/TiO₂ NPs, the inhibition zone was determined in mm (Fig. 13) after 24 h of incubation, and the ranges were determined to be 9, 12, 16, 20, and 22 mm, respectively, in width. When the Au NPs/TiO₂ NP concentrations were 1, 2, 4, 8, and 16 mg/ml in gram-negative *Escherichia coli*, the mean values for zone inhibition were 8, 12, 14, 18, and 20 mm, respectively. The AuNPs showed excellent antibacterial activity against all tested isolates (Table 7) and Figure (14) a. This may be because gold is a metal nanomaterial that can be used to treat bacterial infections. The disc diffusion method exhibited the highest antibacterial activity when using 16 mg/mL of gold nanoparticles versus *S. aureus* followed by *E. coli* with a zone of inhibition reaching 22 mm and 20 mm, respectively. The lowest inhibition zone (8 mm) was recorded for *E. coli*. However, the inhibition areas were 16 and 14 mm for *S. aureus* and *E. coli*, when 4 mg/mL of AuNPs was used. In the same manner, the MIC of Au nanoparticles was determined against all the selected bacteria (Table 8). The findings reveal that the Au NPs/TiO₂ NPs shown greater antibacterial activity when compared to the reference medication gentamicin. The MIC was determined as the lowest mean concentration at which microbial growth was completely inhibited.

4. Conclusions

By employing a photodeposition approach to deposit gold nanoparticles over TiO₂ nanoparticles that had been annealed in a N₂ electrode using isopropanol as a sacrificial donor, gold nanoparticle electrodes were created. The circularity of the Au NPs/TiO₂ NPs-N₂ particles is evident in the TEM image. When used in KOH, H₂SO₄, and (2 M KOH+ 0.1 M glycerol) solutions, the gold nanoparticles

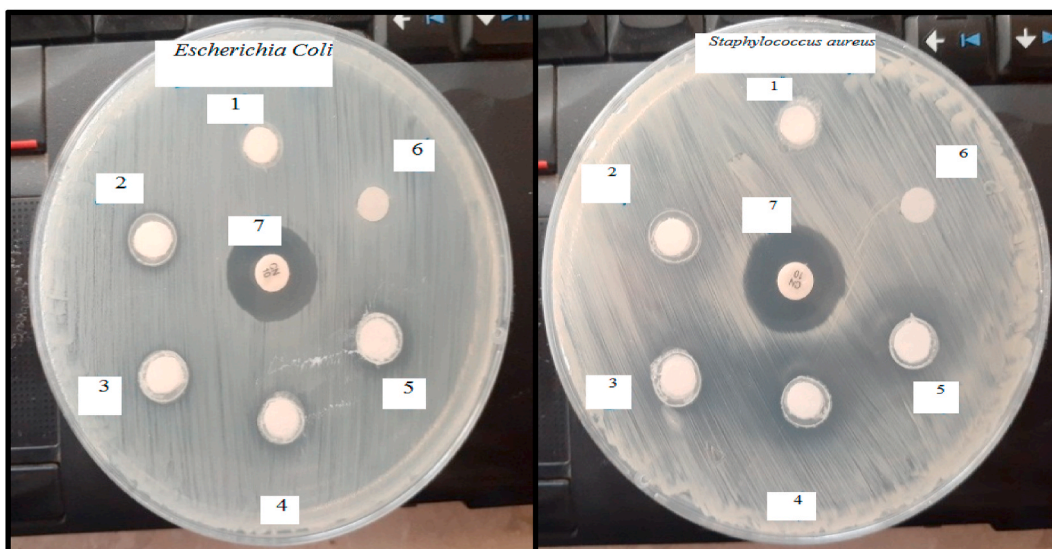


Fig. 11. Antibacterial investigation: zone of inhibition of TiO₂ NPs versus *E. coli* and *S. aureus*.

Table 5

TiO₂ NPs inhibition zone for the two chosen microorganisms was measured in millimeters.

TiO ₂ NPs in mg/ml	Inhibition zone in mm	
	<i>Escherichia coli</i>	<i>Staphylococcus aureus</i>
1	0	9
2	10	11
4	11	12
8	13	14
16	14	17
Control (DMSO)	R ^o	R ^o
Gentamicin (10 µg/ml)	17	18

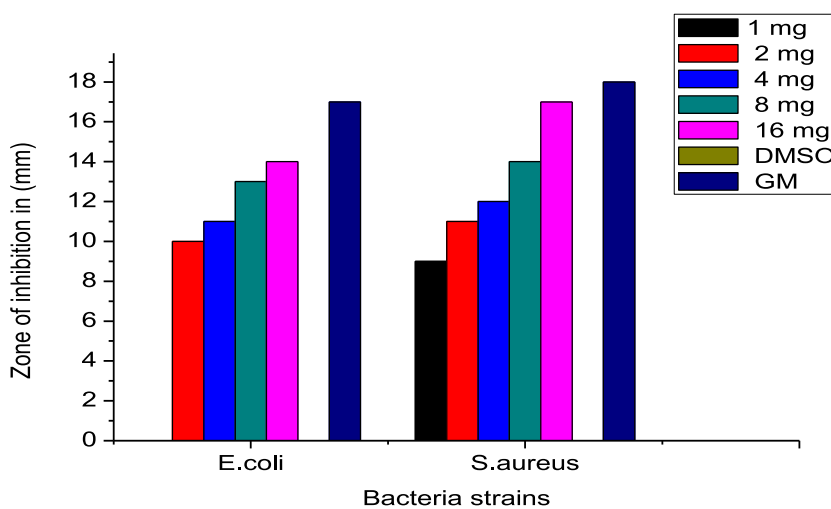


Fig. 12. Comparative inhibition zone of TiO₂ NPs in diameters created vs the bacterial strains that were tested.

outperform commercially available polycrystalline electrodes in terms of electrocatalytic characteristics. Significantly greater currents were observed in the Au NPs/TiO₂ NPs-N₂ electrode in the ferrocyanide system than in the polycrystalline Pt electrode. Au NPs-TiO₂ NPs-N₂ powder electrode can be used as a chloride sensor in an acidic solution (1 M H₂SO₄). These findings demonstrate the potential of Au NPs/TiO₂ NPs-N₂ as electrocatalysts for (GOR) in a basic medium. Gram-positive and Gram-negative human pathogenic

Table 6

The minimum inhibitory concentration (MIC) of TiO₂ NPs versus bacterial strains *E.coli* and *S.aureus*.

Bacteria	MIC in (mg/ml) (average)
<i>Escherichia coli</i>	1.92
<i>Staphylococcus aureus</i>	4.2

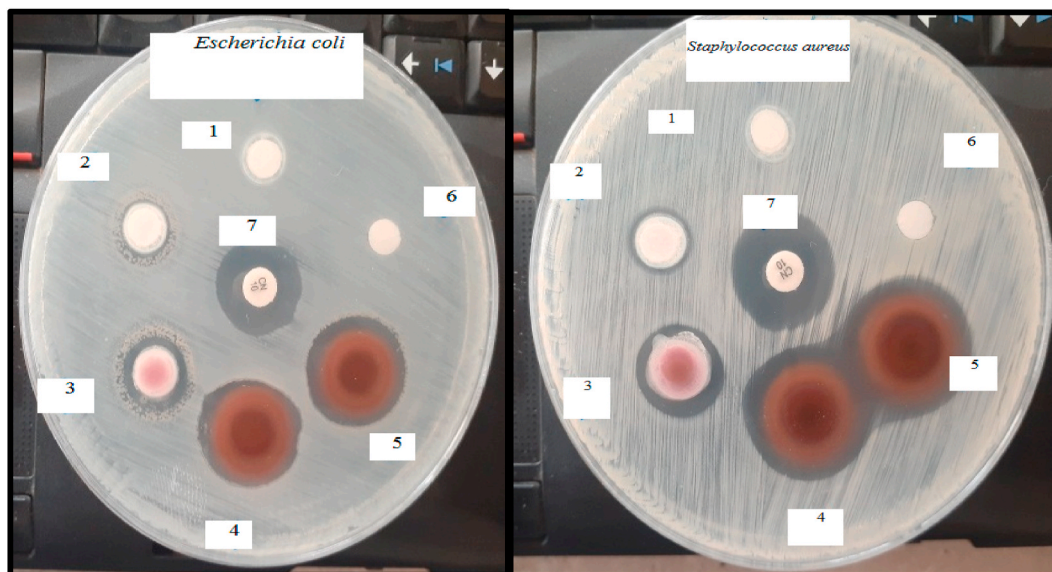


Fig. 13. Antibacterial investigation: inhibition zone of Au NPS/TiO₂ NPs versus *E. coli* and *S. aureus*.

Table 7

The inhibition zone measurement in mm of Au NPS/TiO₂ NPs for the two chosen microorganisms.

Au NPS/TiO ₂ NPs in mg/ml	Inhibition Zone in millimeter	
	<i>Escherichia coli</i>	<i>Staphylococcus aureus</i>
1	8	9
2	12	12
4	14	16
8	18	20
16	20	22
Control (DMSO)	R°	R°
Gentamicin (10 µg/ml)	17	18

microorganisms were evaluated on TiO₂ nanoparticles and Au NPs/TiO₂ NPs. According to the results of this study, both bacteria were more responsive to the antibacterial effects of AuNPs. The studied substances possess antibacterial activity that works differently against the two types of bacteria.

CRedit authorship contribution statement

Hussein M.A. Al-Maydama: Validation, Supervision, Project administration, Methodology. **Yasmin M.S. Jamil:** Writing – review & editing, Writing – original draft, Visualization, Supervision, Software, Project administration, Methodology, Conceptualization. **Mohammed A.H. Awad:** Writing – review & editing, Writing – original draft, Visualization, Validation, Software, Methodology, Investigation, Formal analysis, Data curation, Conceptualization. **Adlia A.M. Abduljabbar:** Visualization, Investigation, Formal analysis.

Declaration of competing interest

The authors declare the following financial interests/personal relationships which may be considered as potential competing interests: Dear Sir, First of all, we would like you to note that Dr. Hussein M.A. Al-Maydama, Dr. Yasmin M.S. Jamil, and Mohammed A.

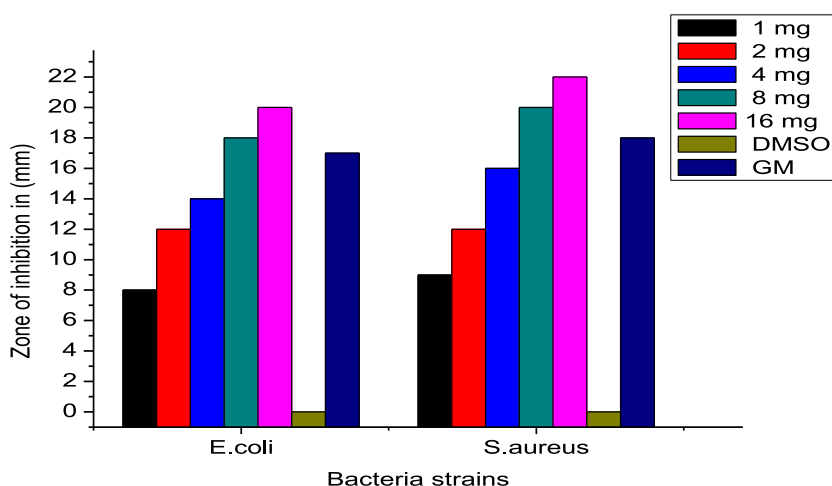


Fig. 14. Comparative inhibition zone of Au NPS/TiO₂ NPs in diameters formed versus the strains of microorganisms examined.

Table 8

The (MIC) of Au NPS/TiO₂ NPs versus bacterium varieties *E. coli* and *S. aureus*.

Bacteria	MIC in (mg/ml) (average)
<i>E. coli</i>	4.11
<i>S. aureus</i>	3.95

H. Awad, Adlia A. M. Abduljabbar are affiliates of Yemen Republic public universities. Mohammed is engaged in the PhD program fully conducted at Sana'a University and this article in the hand is one of his PhD work. Yemen experiencing now a day civil war and is under UN suction. We sought for partial support to finance the PhD program student. Dr. Rabab A. Hakami from SA neighboring country offered to partially finance provided that first, her name should be included in the article as an author, and second the support would be due soon after submitting the paper for publication. However, for some reason, we don't know why Dr. Rabab A. Hakami has failed to honour her offer as promised and consequently, her name was removed from the article. Thank you very much Yours, The Corresponding Author Dr. Yasmin M.S. Jamil.

If there are other authors, they declare that they have no known competing financial interests or personal relationships that could have appeared to influence the work reported in this paper.

References

- [1] Shin-ichi Naya, Miwako Teranishia, Hiroaki Tada, Facile preparation of highly active zirconiasupported gold nanoparticle catalyst, *Catal. Sci. Technol.* (2023), <https://doi.org/10.1039/d3cy00689a>.
- [2] K. Wenderich, G. Mul, Methods, mechanism, and applications of photodeposition in photocatalysis: a review, *Chem. Rev.* 116 (2016) 14587–14619, <https://doi.org/10.1021/acs.chemrev.6b00327>.
- [3] Sawaira Moeen, Muhammad Ikram, Haider Ali, Junaid Haider, Anwar Ul-Hamid, Walid Nabgan, Tahira Shujah, Misbah Naz, Iram Shahzadi, Comparative study of sonophotocatalytic, photocatalytic, and catalytic activities of magnesium and chitosan-doped tin oxide quantum dots, *ACS Omega* 7 (2022) 46428–46439, <https://doi.org/10.1021/acsomega.2c05133>.
- [4] Ayesha Muhammad Imran, Iram Shahzadi, Sawaira Moeen, Anwar Ul-Hamid, Walid Nabgan, Anum Shahzadi, Thamraa Alshahrani, Muhammad Ikram, Polyvinylpyrrolidone and chitosan-coated magnetite (Fe₃O₄) nanoparticles for catalytic and antimicrobial activity with molecular docking analysis, *J. Environ. Chem. Eng.* 11 (3) (2023), 110088, <https://doi.org/10.1016/j.jece.2023.110088>.
- [5] M. Ikram, A. Haider, M. Imran, J. Haider, S. Naz, A. Ul-Hamid, et al., Assessment of catalytic, antimicrobial and molecular docking analysis of starch-grafted polyacrylic acid doped BaO nanostructures, *Int. J. Biol. Macromol.* (2023), <https://doi.org/10.1016/j.ijbiomac.2023.123190>.
- [6] Farzana Jamal, Aqsa Rafique, Sawaira Moeen, Junaid Haider, Walid Nabgan, Haider Ali, Muhammad Imran, Ghazanfar Nazir, Mansur Alhassan, Muhammad Ikram, Qasim Khan, Ghafar Ali, Maaz Khan, Waqas Ahmad, Muhammad Maqbool, Review of metal sulfide nanostructures and their applications, *ACS Appl. Nano Mater.* (2023), <https://doi.org/10.1021/acsnm.3c00417>.
- [7] N. Jadon, R. Jain, S. Sharma, K. Singh, Recent trends in electrochemical sensors for multianalyte detection – a review, *Talanta* 161 (2016) 894–916, <https://doi.org/10.1016/j.talanta.2016.08.084>.
- [8] P. Sierra-Rosales, C. Toledo-Neira, J. Squella, Electrochemical determination of food colorants in soft drinks using MWCNT-modified GCEs, *Sensor. Actuator. B Chem.* 240 (2017) 1257–1264, <https://doi.org/10.1016/j.snb.2016.08.135>.
- [9] Y. Zhang, Q. Wei, The role of nanomaterials in electroanalytical biosensors: a mini review, *J. Electroanal. Chem.* 781 (2016) 401–409, <https://doi.org/10.1016/j.jelechem.2016.09.011>.
- [10] P. Rasheed, N. Sandhyarani, Electrochemical DNA sensors based on the use of gold nanoparticles: a review on recent developments, *Microchim. Acta* 184 (2017) 981–1000, <https://doi.org/10.1007/s00604-017-2143-1>.
- [11] Ö. Yokuş, F. Kardeş, O. Akyıldırım, T. Eren, N. Atar, M. Yola, Sensitive voltammetric sensor based on polyoxometalate/reduced graphene oxide nanomaterial: application to the simultaneous determination of l-tyrosine and l-tryptophan, *Sensor. Actuator. B Chem.* 233 (2016) 47–54, <https://doi.org/10.1016/j.snb.2016.04.050>.

- [12] M. Yola, N. Atar, A highly efficient nanomaterial with molecular imprinting polymer: carbon nitride nanotubes decorated with graphene quantum dots for sensitive electrochemical determination of chlorpyrifos, *J. Electrochem. Soc.* 164 (2017) B223–B229, <https://doi.org/10.1149/2.1411706jes>.
- [13] S. Narwade, B. Mulik, S. Mali, B. Sathe, Silver nanoparticles sensitized C60(Ag@C60) as efficient electrocatalysts for hydrazine oxidation: implication for hydrogen generation reaction, *Appl. Surf. Sci.* 396 (2017) 939–944, <https://doi.org/10.1016/j.apsusc.2016.11.065>.
- [14] M. Yola, N. Atar, T. Eren, H. Karimi-Maleh, S. Wang, Sensitive and selective determination of aqueous triclosan based on gold nanoparticles on polyoxometalate/reduced graphene oxide nanohybrid, *RSC Adv.* 5 (2015) 65953–65962, <https://doi.org/10.1039/c5ra07443f>.
- [15] M. Yola, T. Eren, N. Atar, A novel and sensitive electrochemical DNA biosensor based on Fe@Au nanoparticles decorated graphene oxide, *Electrochim. Acta* 125 (2014) 38–47, <https://doi.org/10.1016/j.electacta.2014.01.074>.
- [16] M. Yola, N. Atar, Functionalized graphene quantum dots with Bi-metallic nanoparticles composite: sensor application for simultaneous determination of ascorbic acid, dopamine, uric acid and tryptophan, *J. Electrochem. Soc.* 163 (2016) B718–B725, <https://doi.org/10.1149/2.1191614jes>.
- [17] S. Elçin, M. Yola, T. Eren, B. Girgin, N. Atar, Highly selective and sensitive voltammetric sensor based on ruthenium nanoparticle anchored calix[4]amidocrown-5 functionalized reduced graphene oxide: simultaneous determination of quercetin, morin and rutin in grape wine, *Electroanalysis* 28 (2015) 611–619, <https://doi.org/10.1002/elan.201500495>.
- [18] K. Saha, S. Agasti, C. Kim, X. Li, V. Rotello, Gold nanoparticles in chemical and biological sensing, *Chem. Rev.* 112 (2012) 2739–2779, <https://doi.org/10.1021/cr2001178>.
- [19] M. Oyama, Recent nanoarchitectures in metal nanoparticle-modified electrodes for electroanalysis, *Anal. Sci.* 26 (2010) 1–12, <https://doi.org/10.2116/analsci.26.1>.
- [20] M. Yola, N. Atar, A novel voltammetric sensor based on gold nanoparticles involved in p-aminothiophenol functionalized multi-walled carbon nanotubes: application to the simultaneous determination of quercetin and rutin, *Electrochim. Acta* 119 (2014) 24–31, <https://doi.org/10.1016/j.electacta.2013.12.028>.
- [21] H. Erikson, A. Sarapuu, K. Tammeveski, J. Solla-Gullón, J. Feliu, Shape-dependent electrocatalysis: oxygen reduction on carbon-supported gold nanoparticles, *Chemeleurochem* 1 (2014) 1338–1347, <https://doi.org/10.1002/celec.201402013>.
- [22] G. Gotti, K. Fajerwerg, D. Evrard, P. Gros, Electrodeposited gold nanoparticles on glassy carbon: correlation between nanoparticles characteristics and oxygen reduction kinetics in neutral media, *Electrochim. Acta* 128 (2014) 412–419, <https://doi.org/10.1016/j.electacta.2013.10.172>.
- [23] D. Geng, G. Lu, Size effect of gold nanoparticles on the electrocatalytic oxidation of carbon monoxide in alkaline solution, *J. Nano Res.* 9 (2007) 1145–1151, <https://doi.org/10.1007/s11051-007-9210-1>.
- [24] S. Ariana Mirshokraee, M. Muhyuddin, R. Lorenzi, G. Tseberlidis, C. Lo Vecchio, V. Baglio, E. Berretti, A. Lavacchi, C. Santoro, Litchi-derived platinum groupmetal-free electrocatalysts for oxygen reduction reaction and hydrogen evolution reaction in alkaline media, *SusMat* 3 (2023) 248–262, <https://doi.org/10.1002/sus2.121>.
- [25] U. Paulus, A. Wokaun, G. Scherer, T. Schmidt, V. Stamenkovic, V. Radmilovic, et al., Oxygen reduction on carbon-supported Pt–Ni and Pt–Co alloy catalysts, *J. Phys. Chem. B* 106 (2002) 4181–4191, <https://doi.org/10.1021/jp013442l>.
- [26] Yasmin M.S. Jamil, Mohammed A.H. Awad, Hussein M.A. Al-Maydama, Physicochemical properties and antibacterial activity of Pt nanoparticles on TiO₂ nanotubes as electrocatalyst for methanol oxidation reaction, *Results Chem* 4 (2022), 100531, <https://doi.org/10.1016/j.rechem.2022.100531>.
- [27] M. Shao, Electrocatalysis in fuel cells, *Catalysts* 5 (2015) 2115–2121, <https://doi.org/10.3390/catal5042115>.
- [28] Y. Li, Y. Chen, Z.-F. Liu, Circumventing the sabatier principle in electrocatalysis: the case of oxygen reduction reaction on Au(100) in alkaline medium, *ChemRxiv. Cambridge: Cambridge Open Engage.* (2023), <https://doi.org/10.26434/chemrxiv-2023-11q7n>.
- [29] S. Chen, B. Zhang, D. Su, W. Huang, Titania morphology-dependent gold-titania interaction, structure, and catalytic performance of gold/titania catalysts, *ChemCatChem* 7 (2015) 3290–3298, <https://doi.org/10.1002/cctc.201500599>.
- [30] N. Lopez, T.V.W. Janssens, B.S. Clausen, Y. Xu, M. Mavrikakis, T. Bligaard, J.K. Nørskov, On the origin of the catalytic activity of gold nanoparticles for low-temperature CO oxidation, *J. Catal.* 223 (2004) 232–235, <https://doi.org/10.1016/j.jcat.2004.01.001>.
- [31] A. Wieckowski, *Interfacial Electrochemistry*, Routledge, 2017, <https://doi.org/10.1201/9780203750469>.
- [32] T. Fujitani, I. Nakamura, M. Haruta, Role of water in CO oxidation on gold catalysts, *Catal. Lett.* 144 (2014) 1475–1486, <https://doi.org/10.1007/s10562-014-1325-2>.
- [33] R. Camosecco, R. Zanella, Catalytic behavior of gold nanoparticles supported on a TiO₂-Al₂O₃ mixed oxide for CO oxidation at low temperature, *Environ. Sci. Pollut. Res.* 29 (2022), 76992, <https://doi.org/10.1007/s11356-022-21076-2>. –77006.
- [34] F. Conte, I. Rossetti, G. Ramis, C. Vaulot, S. Hajjar-Garreau, S. Bennici, Low metal loading (Au, Ag, Pt, Pd) photo-catalysts supported on TiO₂ for renewable processes, *Materials* 15 (2022) 2915, <https://doi.org/10.3390/ma15082915>.
- [35] S.G. Neophytides, S.H. Zafeiratou, M.M. Jaksic, Selective interactive grafting of composite bifunctional electrocatalysts for simultaneous anodic hydrogen and CO oxidation: I. Concepts and embodiment of novel-type composite catalyst, *J. Electrochem. Soc.* 150 (2003) E512–E526, <https://doi.org/10.1149/1.1606456>.
- [36] J.M. Macak, F. Schmidt-Stein, P. Schmuki, Efficient oxygen reduction on layers of ordered TiO₂ nanotubes loaded with Au nanoparticles, *Electrochem. Commun.* 9 (2007) 1783–1787, <https://doi.org/10.1016/j.elecom.2007.04.002>.
- [37] M. Momeni, Y. Ghayeb, Fabrication, characterization and photocatalytic properties of Au/TiO₂-WO₃ nanotubular composite synthesized by photo-assisted deposition and electrochemical anodizing methods, *J. Mol. Catal. Chem.* 417 (2016) 107–115, <https://doi.org/10.1016/j.molcata.2016.03.024>.
- [38] M. Momeni, Fabrication of copper decorated tungsten oxide–titanium oxide nanotubes by photochemical deposition technique and their photocatalytic application under visible light, *Appl. Surf. Sci.* 357 (2015) 160–166, <https://doi.org/10.1016/j.apsusc.2015.09.015>.
- [39] M. Momeni, Y. Ghayeb, Cobalt modified tungsten–titanium nanotube composite photoanodes for photoelectrochemical solar water splitting, *J. Mater. Sci. Mater. Electron.* 27 (2015) 3318–3327, <https://doi.org/10.1007/s10854-015-4161-2>.
- [40] S. Angkaew, P. Limsuwan, Preparation of silver-titanium dioxide core-shell (Ag@TiO₂) nanoparticles: effect of Ti-Ag mole ratio, *Procedia Eng.* 32 (2012) 649–655, <https://doi.org/10.1016/j.proeng.2012.01.1322>.
- [41] P. Martins, S. Kappert, H. Nga Le, V. Sebastian, K. Kühn, M. Alves, et al., Enhanced photocatalytic activity of Au/TiO₂ nanoparticles against ciprofloxacin, *Catalysts* 10 (2020) 234, <https://doi.org/10.3390/catal10020234>.
- [42] Z. Bian, T. Tachikawa, W. Kim, W. Choi, T. Majima, Superior electron transport and photocatalytic abilities of metal-nanoparticle-loaded TiO₂ superstructures, *J. Phys. Chem. C* 116 (2012) 25444–25453, <https://doi.org/10.1021/jp309683f>.
- [43] B. Katryniok, H. Kimura, E. Skrzyńska, J. Girardon, P. Fongarland, M. Capron, et al., Selective catalytic oxidation of glycerol: perspectives for high value chemicals, *Green Chem.* 13 (2011) 1960, <https://doi.org/10.1039/c1gc15320j>.
- [44] H. Kim, S. Choi, S. Green, G. Tompsett, S. Lee, G. Huber, et al., Highly active and stable PtRuSn/C catalyst for electrooxidations of ethylene glycol and glycerol, *Appl. Catal. B Environ.* 101 (2011) 366–375, <https://doi.org/10.1016/j.apcatb.2010.10.005>.
- [45] M. Simões, S. Baranton, C. Coutanceau, Electro-oxidation of glycerol at Pd based nano-catalysts for an application in alkaline fuel cells for chemicals and energy cogeneration, *Appl. Catal. B Environ.* 93 (2010) 354–362, <https://doi.org/10.1016/j.apcatb.2009.10.008>.
- [46] Z. Zhang, L. Xin, W. Li, Electrochemical oxidation of glycerol on Pt/C in anion-exchange membrane fuel cell: cogeneration of electricity and valuable chemicals, *Appl. Catal. B Environ.* 119–120 (2012) 40–48, <https://doi.org/10.1016/j.apcatb.2012.02.009>.
- [47] B. Zope, D. Hibbitts, M. Neurock, R. Davis, Reactivity of the gold/water interface during selective oxidation catalysis, *Science* 330 (2010) 74–78, <https://doi.org/10.1126/science.1195055>.
- [48] S. Carrettin, P. McMorn, P. Johnston, K. Griffin, G. Hutchings, Selective oxidation of glycerol to glyceric acid using a gold catalyst in aqueous sodium hydroxide, *Chem* (2002) 696–697, <https://doi.org/10.1039/b201112n>.
- [49] M. Pagliaro, R. Ciriminna, H. Kimura, M. Rossi, C. Della Pina, From glycerol to value-added products, *Angew. Chem., Int. Ed.* 46 (2007) 4434–4440, <https://doi.org/10.1002/anie.200604694>.
- [50] R. Tripathi, A. Shrivastav, B. Shrivastav, Biogenic gold nanoparticles: as a potential candidate for brain tumor directed drug delivery, *Artificial Cells, Nanomed, Biotechnol.* 43 (2014) 311–317, <https://doi.org/10.3109/21691401.2014.885445>.

- [51] S. Donga, G. Bhadu, S. Chanda, Antimicrobial, antioxidant and anticancer activities of gold nanoparticles green synthesized using *Mangifera indica* seed aqueous extract, *Artificial Cells, Nanomed. Biotechnol.* 48 (2020) 1315–1325, <https://doi.org/10.1080/21691401.2020.1843470>.
- [52] F. Milanezi, L. Meireles, M. de Christo Scherer, J. de Oliveira, A. da Silva, M. de Araujo, et al., Antioxidant, antimicrobial and cytotoxic activities of gold nanoparticles capped with quercetin, *Saudi Pharmaceut. J.* 27 (2019) 968–974, <https://doi.org/10.1016/j.jsps.2019.07.005>.
- [53] R. Vijayan, S. Joseph, B. Mathew, Anticancer, antimicrobial, antioxidant, and catalytic activities of green-synthesized silver and gold nanoparticles using *Bauhinia purpurea* leaf extract, *Bioproc. Biosyst. Eng.* 42 (2018) 305–319, <https://doi.org/10.1007/s00449-018-2035-8>.
- [54] A. Chahardoli, N. Karimi, F. Sadeghi, A. Fattahi, Green approach for synthesis of gold nanoparticles from *Nigella arvensis* leaf extract and evaluation of their antibacterial, antioxidant, cytotoxicity and catalytic activities, *Artificial Cells, Nanomed. Biotechnol.* 46 (2017) 579–588, <https://doi.org/10.1080/21691401.2017.1332634>.
- [55] E. Ahn, S. Hwang, M. Choi, S. Cho, H. Lee, Y. Park, Upcycling of jellyfish (*Nemopilema nomurai*) sea wastes as highly valuable reducing agents for green synthesis of gold nanoparticles and their antitumor and anti-inflammatory activity, *Artificial Cells, Nanomed. Biotechnol.* 46 (2018) 1127–1136, <https://doi.org/10.1080/21691401.2018.1480490>.
- [56] Anum Shahzadi, Sawaira Moeen, Aryan Dilawar Khan, Haider Ali, Junaid Haider, Anwar Ul-Hamid, Walid Nabgan, Iram Shahzadi, Muhammad Ikram, Ali Al-Shanini, La-Doped CeO₂ Quantum Dots: Novel Dye Degradation, Antibacterial Activity, and *in Silico* Molecular Docking Analysis, *ACS Omega*, 2023, <https://doi.org/10.1021/acsomega.2c07753>.
- [57] M. Ikram, A. Haider, M. Imran, J. Haider, S. Naz, A. Ul-Hamid, A. Shahzadi, S. Moeen, G. Nazir, W. Nabgan, A. Bashir, Cellulose grafted poly acrylic acid doped manganese oxide nanorods as novel platform for catalytic, antibacterial activity and molecular docking analysis, *Surface. Interfac.* 37 (2023), 102710, <https://doi.org/10.1016/j.surfint.2023.102710>.
- [58] Muhammad Ikram, Haider Ali, Syeda Tayaba Bibi, Anwar Ul-Hamid, Junaid Haider, Iram Shahzadi, Walid Nabgan, Sawaira Moeen, a Salam Ali, Souraya Goumri-Said, Mohammed Benali Kanoun, Synthesis of Al/starch co-doped in CaO nanoparticles for enhanced catalytic and antimicrobial activities: experimental and DFT approaches, *RSC Adv.* 12 (2022), 32142, <https://doi.org/10.1039/d2ra06340a>.
- [59] J. Zhao, J. Wang, A.J. Brock, H. Zhu, Plasmonic heterogeneous catalysis for organic transformations, *J. Photochem. Photobiol., C: Photochem. Reviews.* 52 (2022), 100539, <https://doi.org/10.1016/j.jphotochemrev.2022.100539>.
- [60] M.D. Hernández-Alonso, F. Fresno, S. Suárez, J.M. Coronado, Development of alternative photocatalysts to TiO₂: challenges and opportunities, *Energy Environ. Sci.* 2 (2009) 1231–1257, <https://doi.org/10.1039/b907933e>.
- [61] H. Chen, L. Wang, Nanostructure sensitization of transition metal oxides for visible-light photocatalysis, *Beilstein J. Nanotechnol.* 5 (2014) 696–710, <https://doi.org/10.3762/bjnano.5.82>.
- [62] D.B. Ingram, S. Lincic, Water splitting on composite plasmonic metal/semiconductor photoelectrodes: evidence for selective plasmon-induced formation of charge carriers near the semiconductor surface, *J. Am. Chem. Soc.* 133 (2011) 5202–5205, <https://doi.org/10.1021/ja200086g>.
- [63] L. Jiang, G. Zhou, J. Mi, Z. Wu, Fabrication of visible-light-driven one-dimensional anatase TiO₂/Ag heterojunction plasmonic photocatalyst, *Catal. Commun.* 24 (2012) 48–51, <https://doi.org/10.1016/j.catcom.2012.03.017>.
- [64] Bani, Fathima John, M. Sharfudeen, Afrin Fathima, Abdul Latheef, Rose, Venis Ambrose, Synthesis and characterization of TiO₂ nanoparticles and investigation of antimicrobial activities against human pathogens, *J. Pharmaceut. Sci. Res.* 9 (2017) 1604–1608. ISSN:0975-1459, <https://www.jpsr.pharmainfo.in>.
- [65] V. Ramkumar, A. Pugazhendhi, K. Gopalakrishnan, P. Sivagurunathan, G. Saratale, T. Dung, et al., Biofabrication and characterization of silver nanoparticles using aqueous extract of seaweed *Enteromorpha compressa* and its biomedical properties, *Biotechnol. Rep.* 14 (2017) 1–7, <https://doi.org/10.1016/j.btre.2017.02.001>.
- [66] P. Pitchai, P. Subramani, R. Selvarajan, R. Sankar, R. Wilwanathan, T. Sibanda, Green synthesis of gold nanoparticles (AuNPs) using *Caulerpa racemosa* and evaluation of its antibacterial and cytotoxic activity against human lung cancer cell line, *Arab. J. Basic Appl. Sci.* 29 (1) (2022) 351–362, <https://doi.org/10.1080/25765299.2022.2127510>.
- [67] Yasmin M.S. Jamil, Mohammed Ahmed Hussein Awad, Hussein M.A. Al-Maydama, Ahmed N. Alhakimi, Mohamad M.E. Shakhofa, Samir Osman Mohammed, Gold nanoparticles loaded on TiO₂ nanoparticles doped with N₂ as an efficient electrocatalyst for glucose oxidation: preparation, characterization, and electrocatalytic properties, *J. Anal. Sci. Technol.* 13 (54) (2022), <https://doi.org/10.1186/s40543-022-00363-0>.
- [68] V. González, B. Kharisov, I. Gómez, Preparation, optical characterization and stability of gold nanoparticles by facile methods, *Rev. Mexic. Fisica* 65 (2019) 690–698, <https://doi.org/10.31349/RevMexFis.65.690>.
- [69] V. Pifferi, A. Testolin, C. Ingrosso, M. Lucia Curri, I. Palchetti, L. Falcicola, Au nanoparticles decorated graphene-based hybrid nanocomposite for as(III) electroanalytical detection, *Chemosensors* 10 (2022) 67, <https://doi.org/10.3390/chemosensors10020067>.
- [70] H. Cheng, Application of gold nanoparticles and nano-diamond modified electrode for hemoglobin electrochemistry, *Int. J. Electrochem. Sci.* 15 (2020) 11416–11426, <https://doi.org/10.20964/2020.11.15>.
- [71] W. Wang, J. Chen, Z. Zhou, S. Zhan, Z. Xing, H. Liu, L. Zhang, Ultrasensitive and selective detection of glutathione by ammonium carbamate–gold platinum nanoparticles-based electrochemical sensor, *Life* 12 (2022) 1142, <https://doi.org/10.3390/life12081142>.
- [72] A. Alshammari, S. Ganash, E. Development of a novel electrochemical sensor based on gold nanoparticles modified carbon-paste electrode for the detection of Congo red dye, *Molecules* 28 (2023) 19, <https://doi.org/10.3390/molecules28010019>.
- [73] Mir, Ghasem Hosseini, Mohamad Mohsen Momeni, Solmaz Zeynali, Au nanoparticle-doped TiO₂ nanotubes catalysts prepared by anodizing and electroplating methods and its application for nitrite detection, *J. Mater. Sci. Eng. B* 2 (1) (2012) 16–23.
- [74] I. Georgiana Munteanu, C. Apetrei, Tyrosinase-based biosensor—a new tool for chlorogenic acid detection in nutraceutical formulations, *Materials* 15 (2022) 3221, <https://doi.org/10.3390/ma15093221>.
- [75] C. Lamy, C. Coutanceau, S. Baranton, Production of hydrogen by the electrocatalytic oxidation of low-weight compounds (HCOOH, MeOH, EtOH), in: *Production of Clean Hydrogen by Electrochemical Reforming of Oxygenated Organic Compounds*, Elsevier, 2020, pp. 37–79, <https://doi.org/10.1016/b978-0-12-821500-5.00004-7>.
- [76] B. Wang, L. Tao, Y. Cheng, F. Yang, Y. Jin, C. Zhou, et al., Electrocatalytic oxidation of small molecule alcohols over Pt, Pd, and Au catalysts: the effect of alcohol's hydrogen bond donation ability and molecular structure properties, *Catalysts* 9 (2019) 387, <https://doi.org/10.3390/catal9040387>.
- [77] P. Sidambaram, J. Colleran, Nanomole silver detection in chloride-free phosphate buffer using platinum and gold micro- and nanoelectrodes, *J. Electrochem. Soc.* 166 (2019) B532–B541, <https://doi.org/10.1149/2.1371906jes>.
- [78] C. Xiang, Q. Xie, S. Yao, Electrochemical quartz crystal impedance study of glucose oxidation on a nickel hydroxide modified Au electrode in alkaline solution, *Electroanalysis* 15 (2003) 987–990, <https://doi.org/10.1002/elan.200390120>.
- [79] N. Bhuvanendran, S. Ravichandran, S. Kandasamy, H. Su, Ag and Au nanoparticles decorated on synthetic clay functionalized multi-walled carbon nanotube for oxygen reduction reaction, *Appl. Nanosci.* (2021), <https://doi.org/10.1007/s13204-021-01902-8>.
- [80] Y.M.S. Jamil, M.A.H. Awad, H.M.A. Al-Maydama, Y. EL-Ghoul, A.N. Al-Hakimi, Synthesis and study of enhanced electrochemical properties of NiO nanoparticles deposited on TiO₂ nanotubes, *Appl. Organomet. Chem.* 36 (9) (2022), e6795, <https://doi.org/10.1002/aoc.6795>, 1–15.
- [81] U. Schmidt, M. Dönten, J.G. Osteryoung, ChemInform abstract: gold electrocrystallization on carbon and highly oriented pyrolytic graphite from concentrated solutions of LiCl, *ChemInform* 28 (2010), <https://doi.org/10.1002/chin.199743017>.
- [82] A. Ganash, S. Alshammari, E. Ganash, Development of a novel electrochemical sensor based on gold nanoparticles modified carbon-paste electrode for the detection of Congo red dye, *Molecules* 28 (2023) 19, <https://doi.org/10.3390/molecules28010019>.
- [83] M. El-Deab, T. Ohsaka, Hydrodynamic voltammetric studies of the oxygen reduction at gold nanoparticles-electrodeposited gold electrodes, *Electrochim. Acta* 47 (2002) 4255–4261, [https://doi.org/10.1016/s0013-4686\(02\)00487-5](https://doi.org/10.1016/s0013-4686(02)00487-5).
- [84] A. Liu, J. Zhu, J. Han, H. Wu, C. Jiang, Fabrication and characterization of gold nanoclusters on phosphorus incorporated tetrahedral amorphous carbon electrode, *Electrochem. Commun.* 10 (2008) 827–830, <https://doi.org/10.1016/j.elecom.2008.03.012>.
- [85] L. Tu, Gold nanomaterials for biochemical sensing, *Gold Bull.* 55 (2022) 169–185, <https://doi.org/10.1007/s13404-022-00318-8>.

- [86] A.M. Siti Norsafurah, M. Yusairie, J. Khairil Anuar, Synthesis and electrocatalytic activity of Pt/Ni/Ti electrocatalyst for methanol oxidation in alkaline medium, *Aust. J. Basic and Appl. Sci.* 9 (29) (2015) 9–15. <http://www.ajbasweb.com/>.
- [87] Zhiyong Zhang, Xin Le, Wenzhen Li, Supported gold nanoparticles as anode catalyst for anion-exchange membrane-direct glycerol fuel cell (AEM-DGFC), *Int. J. Hydrogen Energy* 37 (2012) 9393–9401, <https://doi.org/10.1016/j.ijhydene.2012.03.019>.
- [88] D. Jeffery, G. Camara, The formation of carbon dioxide during glycerol electrooxidation in alkaline media: first spectroscopic evidences, *Electrochem. Commun.* 12 (2010) 1129–1132, <https://doi.org/10.1016/j.elecom.2010.06.001>.
- [89] H. Razmi, E. Habibi, H. Heidari, Electrocatalytic oxidation of methanol and ethanol at carbon ceramic electrode modified with platinum nanoparticles, *Electrochim. Acta* 53 (2008) 8178–8185, <https://doi.org/10.1016/j.electacta.2008.06.033>.
- [90] S. M, B. K, B. M, J. S, A. S, S. A, et al., Obtaining titanium dioxide nanoparticles with spherical shape and antimicrobial properties using *M. citrifolia* leaves extract by hydrothermal method, *J. Photochem. Photobiol. B Biol.* 171 (2017) 117–124, <https://doi.org/10.1016/j.jphotobiol.2017.05.003>.
- [91] V. Ramalingam, S. Revathidevi, T. Shanmuganayagam, L. Muthulakshmi, R. Rajaram, Gold nanoparticle induces mitochondria-mediated apoptosis and cell cycle arrest in nonsmall cell lung cancer cells, *Gold Bull.* 50 (2017) 177–189, <https://doi.org/10.1007/s13404-017-0208-x>.